Aptamer-Conjugated Graphene Oxide Membranes for Highly Efficient Capture and Accurate Identification of Multiple Types of Circulating Tumor Cells

Bhanu Priya Viraka Nellore, Rajashekhar Kanchanapally, Avijit Pramanik, Sudarson Sekhar Sinha, Suhash Reddy Chavva, Ashton Hamme, II, and Paresh Chandra Ray*

Department of Chemistry and Biochemistry, Jackson State University, Jackson, Mississippi 39217, United States

ABSTRACT: Tumor metastasis is responsible for 1 in 4 deaths in the United States. Though it has been well-documented over past two decades that circulating tumor cells (CTCs) in blood can be used as a biomarker for metastatic cancer, there are enormous challenges in capturing and identifying CTCs with sufficient sensitivity and specificity. Because of the heterogeneous expression of CTC markers, it is now well understood that a single CTC marker is insufficient to capture all CTCs from the blood. Driven by the clear need, this study reports for the first time highly efficient capture and accurate identification of multiple types of CTCs from infected blood using aptamer-modified porous graphene oxide membranes. The results demonstrate that dye-modified S6, A9, and YJ-1 aptamers attached to 20−40 μm porous garphene oxide membranes are capable of capturing multiple types of tumor cells (SKBR3 breast cancer cells, LNCaP prostate cancer cells, and SW-948 colon cancer cells) selectively and simultaneously from infected blood. Our result shows that the capture efficiency of graphene oxide membranes is ∼95% for multiple types of tumor cells; for each tumor concentration, 10 cells are present per milliliter of blood sample. The selectivity of our assay for capturing targeted tumor cells has been demonstrated using membranes without an antibody. Blood infected with different cells also has been used to demonstrate the targeted tumor cell capturing ability of aptamer-conjugated membranes. Our data also demonstrate that accurate analysis of multiple types of captured CTCs can be performed using multicolor fluorescence imaging. Aptamer-conjugated membranes reported here have good potential for the early diagnosis of diseases that are currently being detected by means of cell capture technologies.
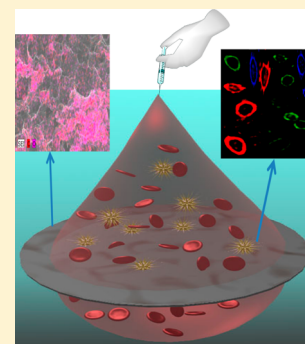
■ INTRODUCTION

According to the American Cancer Society (ACR), 1 in 4 deaths in the United States is caused by cancer.[1,2] As per 2014 cancer statistics, tumor metastasis is responsible for >90% of cancer-related deaths.[1,2] Metastasis happens when tumor cells escape from the primary tumor site and enter into the bloodstream, which is known as circulating tumor cells (CTCs).[3−8] Recently, several clinical studies have reported that the amount of CTCs in blood can be used to correlate the clinical outcome in patients with metastatic breast, prostate, colorectal, and lung cancer.[9−14] Because CTCs are the precursors of metastasis, accurate quantification of CTCs in the bloodstream is very important, and it is the key for the overall survival of cancer patients.[15−17] Although CTCs were first discovered more than 150 years ago, because CTCs are extremely rare epithelial cells (1−10 cells/mL) present in blood of patients with advanced cancer, until now it has been a real challenge to capture CTCs from patients with early stage cancer.[5−12] Because of the general assumption that the CTC originated from an epithelial solid tumor, most of the currently available detection methods, including CellSearch that is approved by the Food and Drug Administration (FDA), used epithelial cell adhesion molecule (EpCAM) antibodies to capture CTC from cancer patients.[5−15] However, several recent reports show that because of tumor heterogeneity and the fact CTCs frequently lose their epithelial nature upon epithelial−mesenchymal transition (EMT), the detection and enrichment of CTCs based on EpCAM often encounter major challenges.[2,3,7,8] As a result, several clinical studies have indicated that more than one-third of patients with metastatic disease do not have detectable CTCs as determined by EpCAM-based technology.[3,7,8] Even these reports indicated that patients with undetectable CTCs have a more favorable prognosis than patients with detectable CTCs.[3,7,8] From all the data reported in the studies mentioned above, it is clear that a single CTC marker will be insufficient to provide a complete account of CTCs. Driven by the clear need, in this work, we report for the first time the highly efficient capture and accurate identification of multiple types of CTCs using porous graphene oxide membranes, as shown in Scheme 1.

Because of the high-yield production, low cost, and interesting electronic and optical properties,[18−28] graphene and its derivative graphene oxide hold great promise for real life applications.[29−38] Recent reports indicate that two-dimensional graphene oxide (GO) offers an exciting opportunity to develop new classes of membranes (with a pore size of a few nanometers), which can block all molecules or ions with a hydrated size of >9 Å,[24−31] but because of the smaller pore size,

Scheme 1. (A) Schematic Representation Showing Aptamer-Conjugated Porous Graphene Oxide Membrane-Based Separation and Capture of Multiple Types of CTCs from Infected Blood and (B) Schematic Representation Showing Fluorescence Imaging of Multiple Types of CTCs Captured by Graphene Oxide Membranes Using a Dye-Conjugated Aptamer
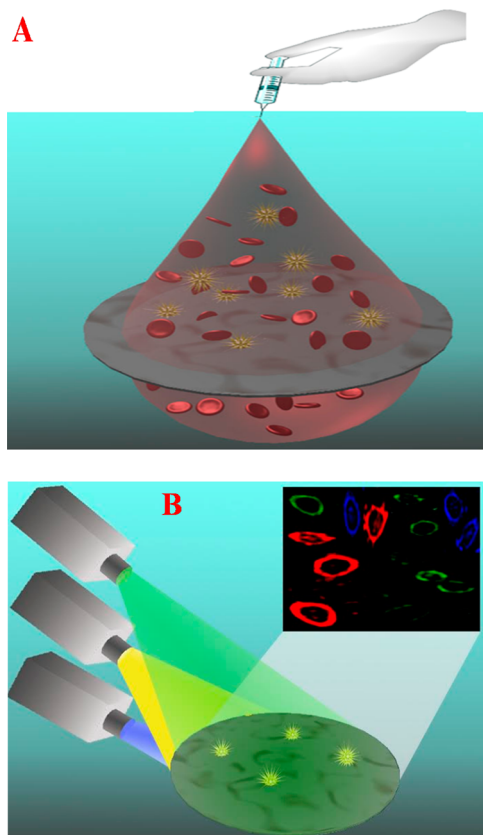
reported membranes cannot be used to filter and capture CTCs from blood samples. The advantage of our novel membranes lies in its porosity size of 20−40 μm, which allows normal red blood cells to travel through the membranes selectively capturing tumor cells because of the presence of different aptamers in three-dimensional (3D) space. To overcome challenges associated with detecting multiple types of rare CTCs in whole blood, we hypothesize that multiple surface markers attached to nanoplatforms are capable of capturing and identifying multiple types of CTCs. The human epidermal growth factor receptor 2 (HER2) biomarker has been shown to be useful for the detection of breast cancer CTCs.[39,40] Similarly, the prostate-specific membrane antigen (PSMA) biomarker has been proven to be very useful for the detection of CTCs from prostate cancer patients.[41,42] On the other hand, the carcinoembryonic antigen (CEA) biomarker has been used to detect colon cancer CTCs.[43] To assess multiple types of cancer-specific biomarkers (CEA, HER-2, and PSMA), we have developed porous graphene oxide membranes attached to several different types of aptamers. To capture different types of tumor cells selectively and simultaneously, three different types of aptamers are used. The S6 aptamer that binds specifically to HER2,[39,40] the A9 aptamer that binds specifically to PSMA,[41,42] and the YJ-1 aptamer that binds to CEA[43] were covalently attached to porous membranes. In our design, we have used 3D graphene oxide foam as the macro-scaffold because of its

microporosity, huge surface area, strong mechanical strength, and very good biocompatibility.[38] Our reported result shows that aptamer-conjugated porous garphene oxide membranes are capable of capturing SKBR3 breast cancer cells, LNCaP prostate cancer cells, and SW-948 colon cancer cells separately and simultaneously from infected blood. It is now well documented that graphene oxide can act as a very highly efficient quencher,[12,25,32,34] and as a result, when dye-conjugated aptamers are attached to graphene oxide, fluorescence from dye is totally quenched by graphene oxide. In the presence of targeted cancer cells, because cancer cells bind to the dye-conjugated aptamer, the distance between the dye and graphene oxide increases, and as a result, fluorescence persists. Our results demonstrate that the Alexa Fluor 488 dye-modified YJ-1 aptamer-conjugated, Cy2-modified S6 aptamer-conjugated, and Cy5-modified A9 aptamer-conjugated graphene oxide membranes are not only capable of capturing different types of cancer cells but also capable of accurately identifying the captured cancer cells via multicolor fluorescence imaging.

RESULTS AND DISCUSSION

For highly efficient capture and accurate identification, we have developed aptamer-attached 3D graphene oxide foam-based membranes. For this purpose, at first we produced two-dimensional (2D) graphene oxide sheets using a modified Hummers method, as we have reported recently.[34−36]

In next step, we attached four different types of aptamers with 2D graphene oxide, and for this purpose, 3′-NH- and 5′-dye-modified aptamers were attached with 2D graphene oxide via the carboxyl group, as shown in Figure 1A.[34−36] For accurate identification, we used the Alexa Fluor 488 dye-modified YJ-1 aptamer, which can specifically capture SW-948 colon cancer cells from infected blood and can be identified via blue fluorescence imaging. We also used the Cy2-modified S6 aptamer, which can specifically bind SK-BRr3 breast cancer cells and can be identified via red fluorescence imaging. Similarly, we used the Cy5-modified A9 aptamer for specific capturing of LNCaP prostate cancer cells from blood sample, and they can be identified via red fluorescence imaging. In next step, 3D graphene oxide foam was developed from aptamer-attached 2D graphene oxide using PEG as a cross-linking agent, as shown in Figure 1A. In our design, amine-functionalized PEG was used to form the 3D porous architecture by interconnecting the graphene oxide sheets via amine groups. We have used coupling chemistry between the -CO₂H group of 2D graphene oxide and the -NH₂ group of PEG to form 3D material from 2D hybrid graphene oxide. For this purpose, EDC {1-ethyl-3-[3-(dimethylamino)propyl]carbodiimide} was used as a cross-linking agent to couple carboxyl groups to amines. Next, the resulting semisolid was spin-casted to yield a final membrane diameter of around 5 cm, which was used for further characterization, as shown in Figure 1B. Panels C and D of Figure 1 display high-resolution scanning electron microscope (SEM) images with energy-dispersive X-ray spectroscopy (EDX) mapping of the membrane's microstructure, which shows an interconnected 3D network with a pore size of 20−40 μm. EDX mapping clearly shows the presence of C and O in the 3D hybrid graphene oxide network. Using nitrogen adsorption analysis via the Brunauer−Emmett−Teller (BET) method, we found that the specific surface area for the 3D hybrid graphene oxide-based membranes was 580 m² g⁻¹, and the pore volume was 0.620 cm³ g⁻¹. Via BET analysis, we
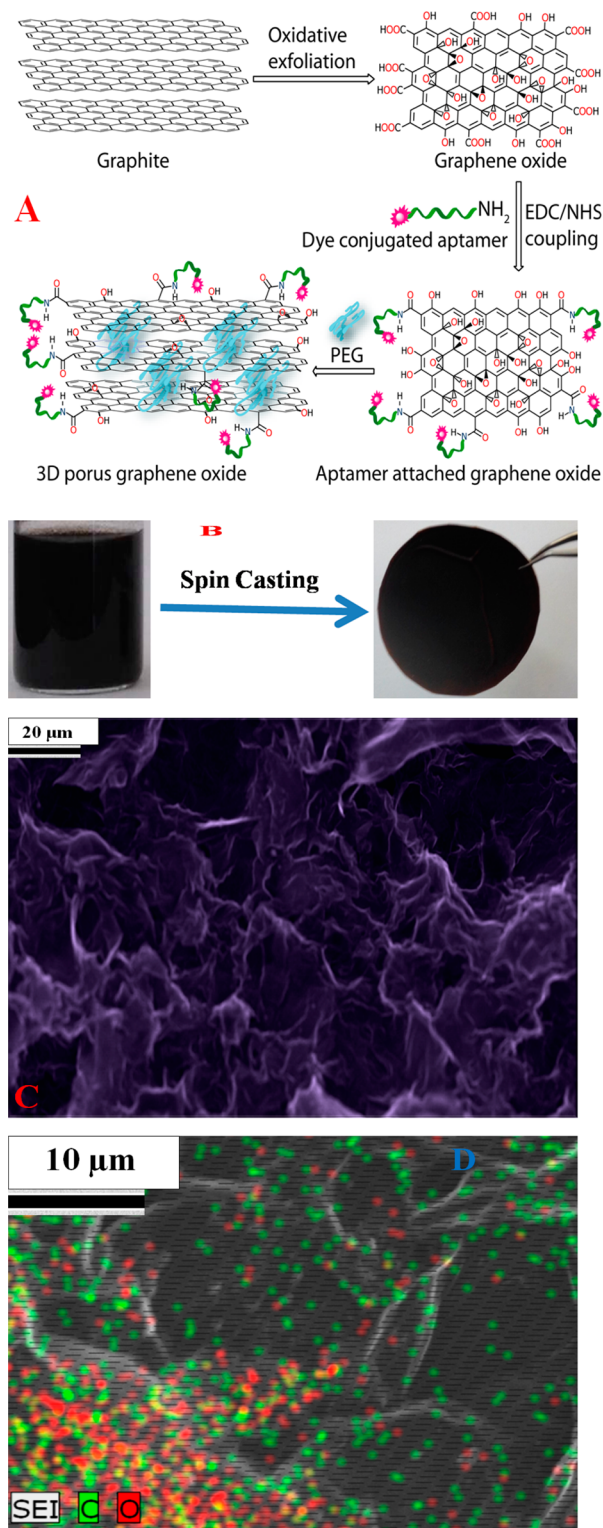
Figure 1. (A) Schematic representation showing the stepwise chemical formation of 3D graphene oxide. (B) Photograph showing the formation of a porous graphene oxide membrane from aptamer-bound graphene oxide foam. (C) Scanning electron microscopy image of a graphene oxide membrane, which indicates a pore size of 20–40 μm. (D) Energy-dispersive X-ray spectroscopy mapping showing the presence of C and O in 3D network membranes.

measured the pore size distribution, which shows an average pore diameter of 25 μm.

To determine whether our aptamer-attached 3D graphene oxide foam-based membranes can be used for tumor cell analysis in settings close to clinical diagnosis, different concentrations of cancer cells were spiked into 10 mL of citrated whole rabbit blood. After the blood had been gently shaken for 90 min, we filtered the infected blood sample using our membrane. Next, tumor cell-attached membranes and the supernatant blood sample were characterized using enzyme-linked immunosorbent assay (ELISA) analysis and fluorescence and transmission electron microscopy (TEM) image analysis as shown in Figures 2–4. To determine how selective the membranes with respect to capturing targeted tumor cells, we performed experiments using membranes without the YJ-1 aptamer, as a negative control. For this purpose, we developed membranes with and without the Alexa Fluor 488 dye-modified YJ-1 aptamer. We also used LNCaP prostate cancer cell-infected blood as a negative control. Using an ELISA, we found that the amount of CEA in SW-948 colon cancer cells was 1.2 × 10^6 cell^{-1}, but no CEA was found in blood cells or LNCaP cells. As a result, we used SW-948 colon cancer cell-infected blood for a targeted cancer cell capture experiment and LNCaP prostate tumor cell-infected blood as a negative control experiment.

Next, we used a blood sample infected with SW-948 colon cancer cells (100 cells/mL) to determine the capture efficiency of membranes in the presence and absence of the YJ-1 aptamer. Figure 2D shows that the capture efficiency of SW-948 colon cancer cells is approximately zero in the absence of aptamer attachment in the membranes. Because the pore size of our novel filer is approximately 20–40 μm, it will allow cells to travel through. On the other, as shown in Figure 2E, ~98% of the colon cancer cells were captured when membranes were attached to YJ-1 aptamers. The TEM image, as shown in Figure 2A, also indicates that SW-948 colon tumor cells are captured by membranes when a YJ-1 aptamer-attached membrane was used. Because of the presence of the YJ-1 aptamer, SW-948 colon cancer cells are selectively captured by membranes via antigen–aptamer interaction.

On the other hand, because of the absence of CEA in blood cells, porous membranes allows normal red blood cells to travel through because of the 20–40 μm pore size. Our experimental data, as shown in Figure 2E, indicate that the colon cancer cell capture efficiency of porous graphene oxide membranes can be ~98%. To visualize the capture of CTC cells, we used a fluorescence microscope. Figure 2C shows the fluorescence image of captured SW-948 colon cancer cells. The blue fluorescence image from SW-948 cancer cells is due to the presence of the Alexa Fluor 488 dye-attached aptamer on the cancer cell surface. Next, to determine whether YJ-1 aptamer-conjugated membranes are selective for targeted colon cancer cell capture, we also performed an experiment using blood infected with LNCaP prostate cancer cells (10^3 cells/mL). As shown in Figure 2F, the ELISA data clearly show that cells were not captured when LNCaP cell-infected blood was used. The fluorescence image shown in Figure 2B also indicates that LNCaP cells are not captured by YJ-1 aptamer-conjugated membranes. All these results clearly show that the membrane's pore size is sufficient for the cells to pass through it, and CTCs are captured by the aptamer only, which indicates that membranes can be used for selective capturing of CTC.

To determine the biocompatibility of our aptamer-attached porous graphene oxide membrane, different tumor cells and HaCaT normal cells (6.4 × 10^4 cells/mL) were incubated
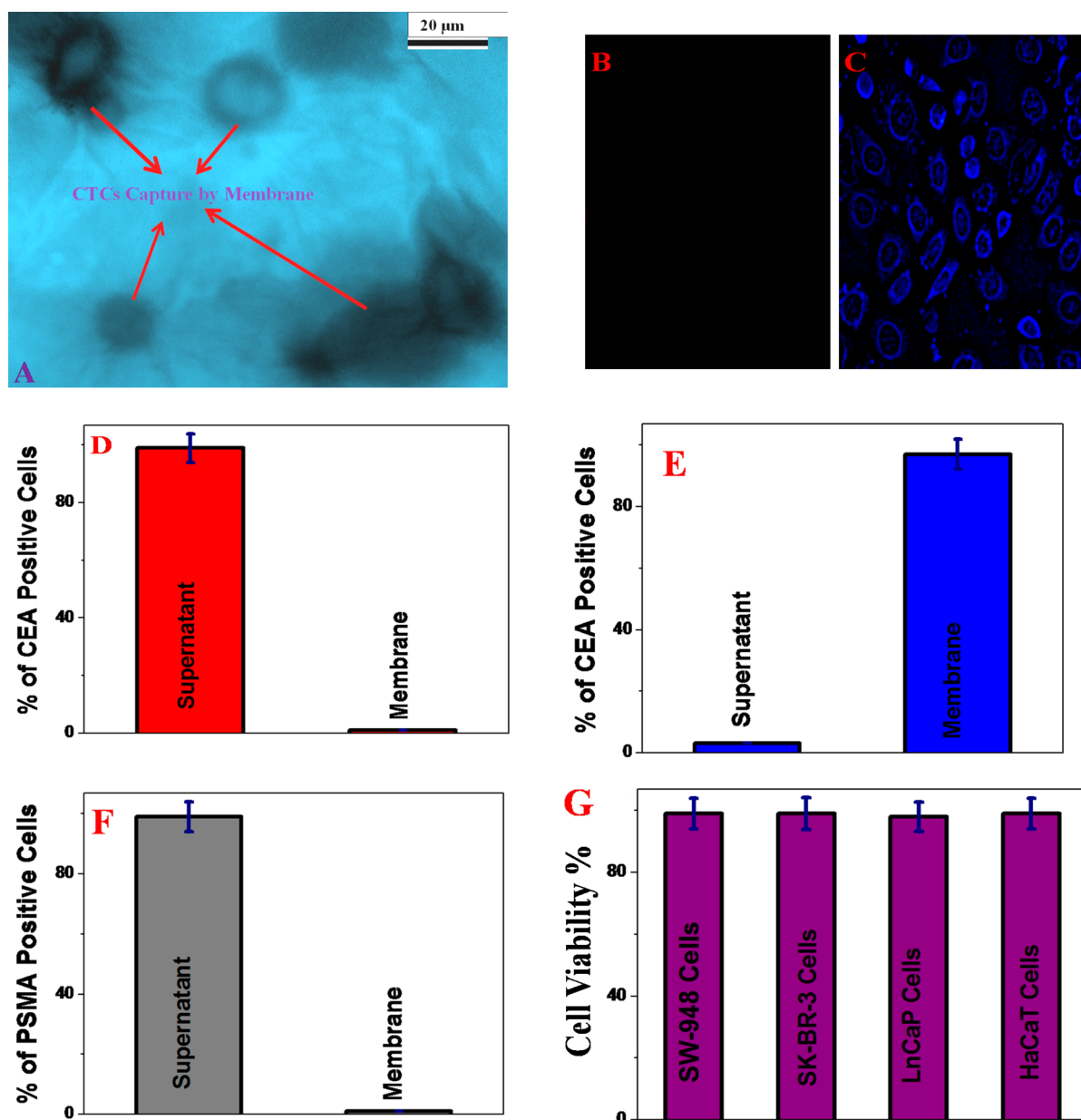
Figure 2. (A) TEM image showing that SW-948 colon tumor cells are captured by the membranes. (B) Fluorescence image showing that LNCaP tumor cells are not captured by the Alexa Fluor 488 dye-modified YJ-1 aptamer-attached membrane. (C) Fluorescence image showing that a huge amount of SW-948 colon tumor cells is captured by the membranes. The observed blue fluorescence is due to the presence of the Alexa Fluor 488 dye-attached aptamer on the SW-948 cancer cell surface. (D) Number of CEA positive cells in the supernatant and membranes in the absence of the YJ-1 aptamer. (E) Number of CEA positive cells in the supernatant and membranes in the presence of the YJ-1 aptamer. (F) Number of PSMA positive cells in the supernatant and membranes when PSMA positive LNCaP colon cancer cell-infected blood was passed through the YJ-1 aptamer-attached membranes. (G) Plot that demonstrates the biocompatibility of our membranes.

separately with membranes for 24 h. After that, the cell viability was measured using the 3-(4,5-dimethylthiazol-2-yl)-2,5-diphenyltetrazolium bromide (MTT) test. Figure 2F clearly shows that even after incubation for 24 h, a cell viability of 97% was observed. All the cytotoxicity results reported above clearly show the very good biocompatibility of the membrane.

Next, to determine how versatile the membrane is for the selective capturing of other tumor cells, we performed an experiment with an SK-BR-3 breast tumor cell-infected blood sample. For this purpose, we developed Cy2-modified S6 aptamer-attached membranes, and afterward, we used the membranes for selective capturing of SK-BR-3 cells from infected blood. ELISA data, as shown in Figure 3C, indicate

that the SK-BR-3 cancer cell capture efficiency of the S6 aptamer-attached membranes can be ∼98%. Using the ELISA kit, we found that the amount of HER2 in SK-BR-3 cells was 4.8×10^6 cell^{-1}, where as no HER2 was found in SW-948 colon cancer cells. As a result, to understand whether S6 aptamer-attached membranes are highly selective for capturing only SK-BR-3 breast tumor cells, we used SW-948 colon cancer cells as a negative control. Figure 3D clearly shows that SW-948 colon cancer cells are not captured by the S6 aptamer-attached membrane, and as a result, all CEA positive cells are in the supernatant. Figure 3A shows the fluorescence image of captured SK-BR-3 breast cancer cells. In the fluorescence image, the observed green fluorescence of SK-BR-3 cells is
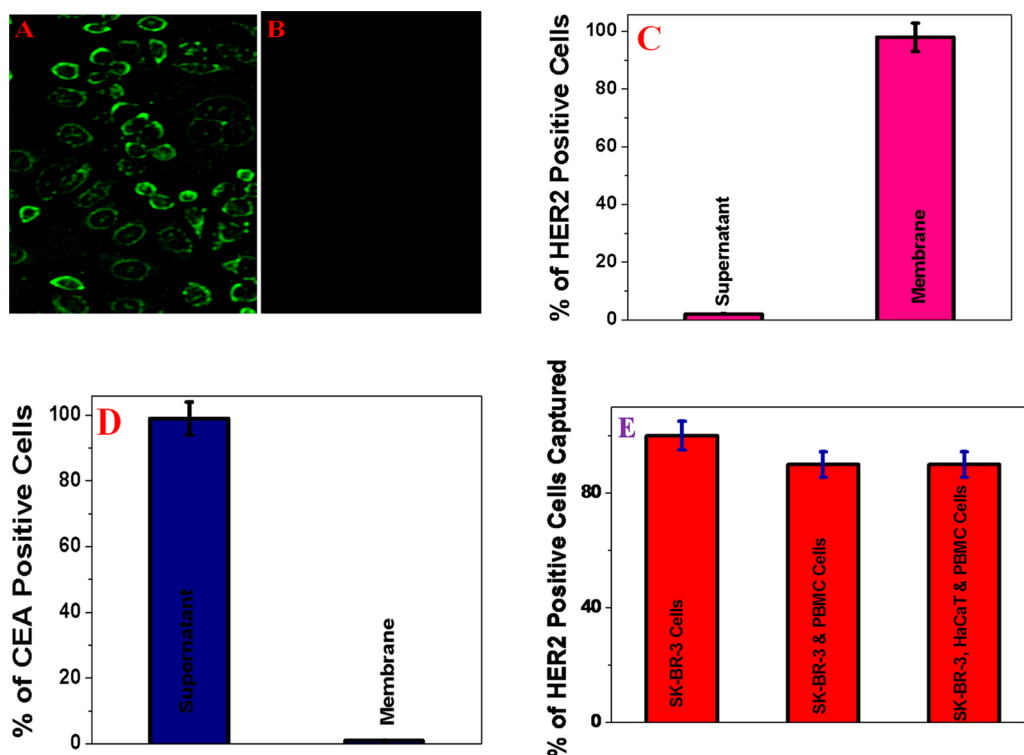
Figure 3. (A) Fluorescence image showing that a huge amount of SK-BR-3 breast cancer cells is captured by the Cy2-modified S6 aptamer-attached membranes. (B) Fluorescence image showing that the capture efficiency is approximately zero when SW-948 colon cancer cell-infected blood is used for capture by the membranes. (C) Number of HER2 positive cells in the supernatant and membranes when HER2 positive SK-BR-3 breast cancer cell-infected blood was passed through the membranes. (D) Number of CEA positive cells in the supernatant and membranes. (E) Percent of HER2 positive cells captured by S6 aptamer-attached membranes, when citrated whole rabbit blood infected with (10 cells/mL) cancerous and (10^5 cells/mL) normal cells was used.

caused by the presence of the Cy2 dye-attached S6 aptamer on the SK-BR-3 breast cancer cell surface. On the other hand, the fluorescence image shown in Figure 3B shows that SW-948 colon cancer cells were not captured by S6 aptamer-attached membranes. Because S6 aptamers are known to selectively bind to HER2, SK-BR-3 breast cancer cells are selectively captured by membranes via HER2−S6 aptamer interaction.

On the other hand, because of the absence of HER2 in blood cells and SW-948 colon cancer cells, porous membranes allow them to travel through. All the experimental data reported above clearly show that S6 aptamer-attached membranes can be used to capture SK-BR-3 breast tumor cells from infected blood.

Because in real life tumor cells coexist with normal cells, to demonstrate that membranes can be used for the capture of tumor cells in a more physiologically relevant system, we performed experiments with a mixture of tumor cells and a normal cell-infected blood sample. For our experiment, citrated whole rabbit blood was infected with tumor cells, peripheral blood mononuclear cells (PBMC), and HaCaT normal skin cells. We kept the concentration the cells in such a way that after mixing, the tumor cell concentration is 10 cells/mL. On the other hand, the concentrations of PBMC and HaCaT cells are both 10^5 cells/mL in infected blood. ELISA data, as shown in Figure 3E, indicate that the SK-BR-3 cancer cell capturing efficiency of the S6 aptamer-attached membranes can be ∼90%, even in the presence of 10^4-fold more PBMC and HaCaT cells each.

Next, to demonstrate that the versatile membranes can be used for capturing of multiple types of tumor cells

simultaneously, we performed experiments with three different tumor cell-infected blood samples. For this purpose, we used a whole blood sample infected with SK-BR-3 breast tumor cells, LNCaP prostate tumor cells, and SW-948 colon cancer cells. The concentration of each tumor cell mixture was kept at 10 cells/mL. For the simultaneous capture of three different types of tumor cells, we developed membranes attached to several cancer cell-specific aptamers. We used the Cy2-bound S6 aptamer that can bind specifically to SK-BR-3 tumor cells because of the presence of HER2, the Cy5-bound A9 aptamer that can bind to LNCaP prostate cancer cells because of the presence of PSMA, and Athe lexa Fluor 488 dye-modified YJ-1 aptamer that can bind to SW-948 colon cancer cells via a carcinoembryonic antigen. ELISA data, as shown in panels C and D of Figure 4, indicate that our membranes have the capability of capturing multiple types of tumor cells and the capturing efficiency of the infected blood sample can be ∼95%.

Figure 4A shows the multicolor fluorescence image, which clearly demonstrates multiple types of tumor cells have been captured by porous graphene oxide membranes. We used a laser scanning microscope to obtain multicolor fluorescence. In the reported fluorescence image, observed red cells are LNCaP prostate cancer cells. Because A9 aptamers are specific to PSAM, LNCaP cells are captured by the Cy5-attached A9 aptamer and the observed red fluorescence is due to the presence of the Cy5-attached aptamer on the prostate cancer cell surface. Similarly, in Figure 4A, captured SK-BR-3 cells are viewed as green cells because of the presence of the Cy2-attached S6 aptamer on the cell surface.
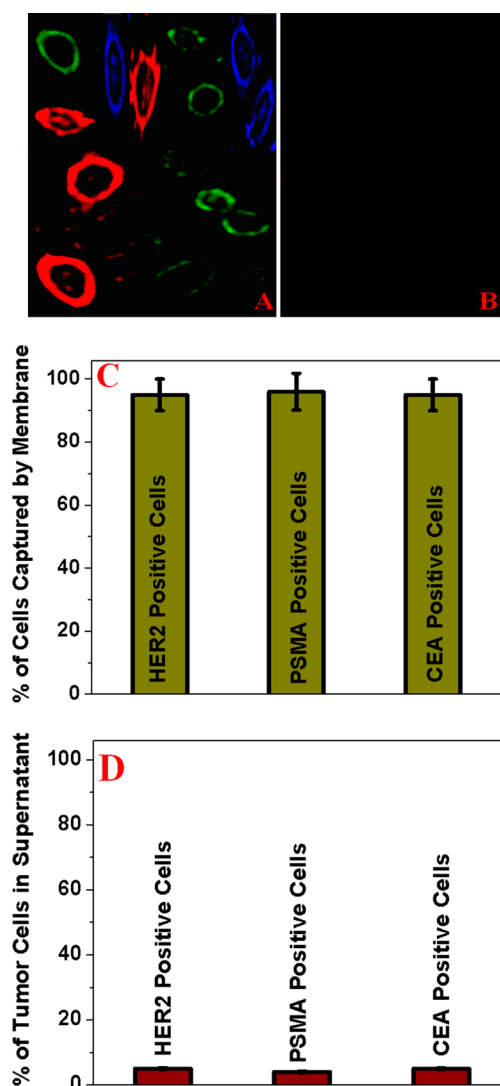
Figure 4. (A) Fluorescence image showing that the bioconjugated porous graphene oxide membrane is capable of capturing different types of tumor cells from infected blood. (B) Fluorescence image demonstrating that no cells are captured when a normal skin HaCaT cell is used. (C) Number of HER2 positive, PSMA positive, and CEA positive cells in membranes. (D) Number of HER2 positive, PSMA positive, and CEA positive cells in the supernatant.

On the other hand, because of the presence of the Alexa Fluor 488 dye-attached YJ-1 aptamer on the SW-948 colon cancer cell surface, in the fluorescence image, captured colon cancer cells are colored blue. Figure 4B shows that no cells are captured when a HaCaT cell-infected blood sample is filtered by three different aptamer-attached porous membranes. All the experimental data provided above clearly show that different aptamer-attached membranes can be used for capturing multiple types of tumor cells from infected blood, and they are highly selective for capturing targeted tumor cells from infected blood.

CONCLUSION

In conclusion, in this article, we have reported very highly efficient removal of multiple types of CTCs from infected blood using aptamer-attached porous graphene oxide membranes. We have developed dye-modified S6, A9, and YJ-1 aptamers attached to 20−40 μm porous garphene oxide

membranes, which are capable of capturing multiple types of tumor cells from infected blood. We have demonstrated that our porous graphene oxide membrane can capture SKBR3 breast cancer cells, LNCaP prostate cancer cells, and SW-948 colon cancer cells selectively and simultaneously from infected blood, with a capture efficiency as high as 98%. Reported experimental data with a porous graphene oxide membrane without an antibody show that the membrane is highly selective for capturing targeted tumor cells. Similarly, assay data using blood infected with different cells confirmed that our assay is highly selective for targeted tumor cell capturing. Our reported data show that multicolor fluorescence imaging can be used for the accurate analysis of multiple types of captured CTCs, which also demonstrate that graphene oxide-based porous membranes can be used for targeted tumor cell capturing. After the proper engineering, the impact of the CTC-captured membranes can go beyond CTC sorting and be used as a fluorescence platform for accurate analysis of targeted CTC. It has good potential for improving the early diagnosis of the disease via cell capture technologies.

◼ EXPERIMENTAL METHODS

We purchased all chemicals, including graphite, $KMnO_4$, PEG, ethylene glycol, and nitric acid, from Fisher Scientific and Sigma-Aldrich. All types of cancer cell lines and HaCaT cell lines and growth media for growing cells were purchased from the American Type Culture Collection (ATCC, Rockville, MD). Dye-modified aptamers were obtained from Midland Certified Reagent Co.

Development of Different Types of Aptamers Attached to 2D Graphene Oxide. We used a reported modified Hummers method for graphite exfoliation by strong oxidizing agents to yield graphene oxide, as we have reported previously.[33−36] For this purpose, 1 g of graphite powder was treated for 30 min with 1 g of $NaNO_3$ in 45 mL of H_2SO_4 and 3 g of $KMnO_4$, without changing the temperature. After the reaction had proceeded for 30 min, a thick paste was obtained. Next, we added water very carefully, drop by drop. After that, we filtered and redispersed the obtained graphene oxide in 100 mL of water and performed sonication for a few hours for the purpose of exfoliation. After that, the acid group was used to connect with 3′-NH- and 5′-dye-modified aptamers. Next, we used a high-resolution JEM-2100F transmission electron microscope to characterize 2D graphene oxide.

Development of 3D Graphene Oxide Foam-Based Membranes. Initially, 3D graphene oxide foam was developed using PEG as a cross-linking agent, as we have reported recently.[38] For this purpose, 10 mL of graphene oxide was added to 20 mg of PEG and then sonicated for 10 min. After being sonicated for 5 min, samples were kept on an oil bath at approximately 80−90 °C, under a hood. The reaction was continued for 40 min. Next, the resulting semisolid 3D graphene oxide foam was used to develop 2 in. diameter membranes using spin-casting, as shown in Figure 1.

Characterization of Nanomaterial Using TEM, SEM, and EDX. 2D and 3D grapahene oxide architectures were characterized using ultra-high-resolution field emission scanning electron microscopy (FE-SEM HITACHI) and a JEOL 2010-F microscope (TEM) using an applied voltage of 200 kV. The scanning electron microscope was coupled with a BF/DF Duo-STEM detector, and EDX spectroscopy (Bruker) was used for EDX analysis.

Cell Culture. Multiple types of cancer cells and normal cells were grown according to the ATCC procedure. SK-BR-3 cells were grown in a a 5% CO_2 incubator at 37 °C using ATCC medium supplemented with 10% premium fetal bovine serum (FBS) and antibiotics (10 IU/mL penicillin G and streptomycin) in 75 cm^2 tissue culture flasks. The HaCaT cells were also grown in Dulbecco's modified Eagle's medium (DMEM), as described by ATCC.

Separation of Tumor Cells from Infected Blood. To demonstrate the possible capturing of tumor cells in a more physiologically relevant system, different concentrations of tumor cells and normal cells were spiked into 10 mL suspensions of citrated whole rabbit blood purchased from Colorado Serum Co. Using ELISA analysis, we found no HER2, CEA, or PSMA present in whole rabbit blood. For our experiment, citrated whole rabbit blood was infected with tumor cells, PBMC, and HaCaT normal skin cells. Using ELISA analysis, we found no HER2, CEA, or PSMA present in PBMC or HaCaT cells. We kept the concentration of each cell in the mixture in such a way that after mixing, the tumor cell concentration was 10 cells/mL. On the other hand, the concentrations of PBMC and HaCaT cells are 10^5 cells/mL each in infected blood. After the blood had been gently shaken for 90 min, we filtered the infected blood sample using our developed membranes. Next, the tumor cell-attached membrane and the supernatant blood sample were characterized by an ELISA and by fluorescence and TEM image analysis as shown in Figures 2−4.

ELISA Assay. The CEA, PSMA, and HER-2 levels were measured using the ELISA kit in accordance with the manufacturer's instructions. We purchased these kits from Anogen, USCN Life Science Inc., and Oncogene Science.

Fluorescence Analysis. We used an Olympus IX71 inverted confocal fluorescence microscope fitted with a SPOT Insight digital camera for fluorescence imaging.

Cell Viability Assay. To study cytotoxicity, cells were treated with nanomaterials at different time intervals, and the cell viability was determined using the MTT assay. For this purpose, 10 μL of nanomaterial was added to 90 μL of cell medium and the mixture incubated for different time intervals at 37 °C with 5% CO_2. Then we added 50 μL of a 5 mg/mL MTT solution and incubated the sample for 60 min. The absorbance at 540 nm was recorded using a Multiskan Ascent Plate Reader with Ascent software (Labsystems).

■ AUTHOR INFORMATION

Corresponding Author
*E-mail: paresh.c.ray@jsums.edu. Fax: +16019793674.

Notes
The authors declare no competing financial interest.

■ ACKNOWLEDGMENTS

■ REFERENCES

(1) Siegel, R., Ma, J., Zou, Z., and Jema, I. A. (2014) Cancer statistics. *Ca-Cancer J. Clin. 64*, 9−29.

(2) Yoon, H. J., Kozminsky, M., and Nagrath, S. (2014) Emerging Role of Nanomaterials in Circulating Tumor Cell Isolation and Analysis. *ACS Nano 8*, 1995−2017.

(3) Allard, W. J., Matera, J., Miller, M. C., Repollet, M., Connelly, M. C., Rao, C., Tibbe, A. G. J., Uhr, J. W., and Terstappen, L. W. M. M. (2004) Tumor Cells Circulate in the Peripheral Blood of All Major Carcinomas but Not in Healthy Subjects or Patients with Non-malignant Diseases. *Clin. Cancer Res. 10*, 6897−6904.

(4) Lohr, J. G., Adalsteinsson, V. A., Cibulskis, K., Choudhury, A. D., Rosenberg, M., Cruz-Gordillo, P., Francis, J. M., Zhang, C. Z., Shalek, A. K., Satija, R., Trombetta, J. J., Lu, D., et al. (2014) Whole-exome sequencing of circulating tumor cells provides a window into metastatic prostate cancer. *Nat. Biotechnol. 32*, 479−484.

(5) Wang, S., Wang, H., Jiao, J., Chen, K. J., Owens, G. E., Kamei, K., Sun, J., Sherman, D. J., Behrenbruch, C. P., Wu, H., and Tseng, H. R. (2009) Three-dimensional nanostructured substrates toward efficient capture of circulating tumor cells. *Angew. Chem., Int. Ed. 48*, 8970−8973.

(6) Yu, M., Bardia, A., Aceto, N., Bersani, F., Madden, M. W., Donaldson, M. C., Desai, R., Zhu, H., Comaills, V., Zheng, Z., Wittner, B. S., et al. (2014) Cancer therapy. Ex vivo culture of circulating breast tumor cells for individualized testing of drug susceptibility. *Science 345*, 216−220.

(7) Wicha, M. S., and Hayes, D. F. (2011) Circulating Tumor Cells: Not All Detected Cells Are Bad and Not All Bad Cells Are Detected. *J. Clin. Oncol. 29*, 1−4.

(8) Yu, M., Bardia, A., Wittner, B. S., Stott, S. L., Smas, M. E., Ting, D. T., Isakoff, S. J., Ciciliano, J. C., Wells, M. N., Shah, A. M., et al. (2013) Circulating Breast Tumor Cells Exhibit Dynamic Changes in Epithelial and Mesenchymal Composition. *Science 339*, 580−584.

(9) Shen, Q., Xu, L., Zhao, L., Wu, D., Fan, Y., Zhou, Y., Ouyang, W. H., Xu, X., Zhang, Z., Song, M., Lee, T., Garcia, M. A., Xiong, B., Hou, S., Tseng, H. R., and Fang, X. (2103) Specific capture and release of circulating tumor cells using aptamer-modified nanosubstrates. *Adv. Mater. 25*, 2368−2373.

(10) Wen, C.-Y., Wu, L.-L., Zhang, Z.-L., Liu, Y.-L., Wei, S.-Z., Hu, J., Tang, M., Sun, E.-Z., Gong, Y.-P., Yu, J., et al. (2014) Quick-Response Magnetic Nanospheres for Rapid, Efficient Capture and Sensitive Detection of Circulating Tumor Cells. *ACS Nano 8*, 941−949.

(11) Lee, S.-K., Kim, G.-S., Wu, Y., Kim, D.-J., Lu, Y., Kwak, M., Han, L., Hyung, J.-H., Seol, J.-K., Sander, C., et al. (2012) Nanowire Substrate-Based Laser Scanning Cytometry for Quantitation of Circulating Tumor Cells. *Nano Lett. 12*, 2697−2704.

(12) Tonga, G. Y., Saha, K., and Rotello, V. M. (2014) 25th Anniversary Article: Interfacing Nanoparticles and Biology: New Strategies for Biomedicine. *Adv. Mater. 26*, 359−370.

(13) Sheng, W., Chen, T., Tan, W., and Fan, Z. H. (2013) Multivalent DNA Nanospheres for Enhanced Capture of Cancer Cells in Microfluidic Devices. *ACS Nano 7*, 7067−7076.

(14) Yoon, H. J., Kim, T. H., Zhang, Z., Azizi, E., Pham, T. M., Paoletti, C., Lin, J., Ramnath, N., Wicha, M. S., Hayes, D. F., et al. (2013) Sensitive Capture of Circulating Tumour Cells by Function-alized Graphene Oxide Nanosheets. *Nat. Nanotechnol. 8*, 735−741.

(15) Liu, Q., Yeh, Y.-C., Rana, S., Jiang, Y., Guo, L., and Rotello, V. M. (2013) Differentiation of Cancer Cell Type and Phenotype Using Quantum Dot-Gold Nanoparticle Sensor Arrays. *Cancer Lett. 334*, 196−201.

(16) Fan, Z., Senapati, D., Singh, A. K., and Ray, P. C. (2013) Theranostic Magnetic Core−Plasmonic Shell Star Shape Nanoparticle for the Isolation of Targeted Rare Tumor Cells from Whole Blood, Fluorescence Imaging, and Photothermal Destruction of Cancer. *Mol. Pharmaceutics 10*, 857−866.

(17) Fan, Z., Shelton, M., Singh, A. K., Senapati, D., Khan, S. A., and Ray, P. C. (2012) Multifunctional Plasmonic Shell−Magnetic Core Nanoparticles for Targeted Diagnostics, Isolation, and Photothermal Destruction of Tumor Cells. *ACS Nano 6*, 1075−1083.

(18) Geim, A. K., and Novoselov, K. S. (2007) The Rise of Graphene. *Nat. Mater. 6*, 183−191.

(19) Li, X., Wang, X., Zhang, L., Lee, S., and Dai, H. (2008) Chemically Derived, Ultrasmooth Graphene Nanoribbon Semi-conductors. *Science 319*, 1229−1232.

(20) Gao, W., Alemany, L. B., Ci, L., and Ajayan, P. M. (2009) New Insights into the Structure and Reduction of Graphite Oxide. *Nat. Chem. 1*, 403−408.

(21) Hossain, M. Z., Johns, J. E., Bevan, K. H., Karmel, H. J., Liang, Y. T., Yoshimoto, S., Mukai, K., Koitaya, T., Yoshinobu, J., et al. (2012) Chemically Homogeneous and Thermally Reversible Oxidation of Epitaxial Graphene. *Nat. Chem. 4*, 305−309.

(22) Sun, P., Zhu, M., Wang, K., Zhong, M., Wei, J., Wu, D., Xu, Z., and Zhu, H. (2013) Selective Ion Penetration of Graphene Oxide Membranes. *ACS Nano 7*, 428−437.

(23) Chou, S. S., De, M., Luo, J., Rotello, V. M., Huang, J., and Dravid, V. P. (2012) Nanoscale Graphene Oxide (nGO) as Artificial Receptors: Implications for Biomolecular Interactions and Sensing. *J. Am. Chem. Soc. 134*, 16725−16733.

(24) Sun, P., Zheng, F., Zhu, M., Song, Z., Wang, K., Zhong, M., Wu, D., Little, R. B., Xu, Z., and Zhu, H. (2014) Selective Trans-Membrane Transport of Alkali and Alkaline Earth Cations through Graphene Oxide Membranes Based on Cation-π Interactions. *ACS Nano 8*, 850−859.

(25) Shi, S., Chen, F., Ehlerding, E. B., and Cai, W. (2014) Surface Engineering of Graphene-Based Nanomaterials for Biomedical Applications. *Bioconjugate Chem. 25*, 1609−1619.

(26) Nair, N. N., Wu, H. A., Jayaram, P. N., Grigorieva, I. V., and Geim, A. K. (2012) Unimpeded Permeation of Water Through Helium-Leak-Tight Graphene-Based Membranes. *Science 335*, 442−444.

(27) Sun, P., Zhu, M., Wang, K., Zhong, M., Wei, J., Wu, D., Xu, Z., and Zhu, H. (2013) Selective Ion Penetration of Graphene Oxide Membranes. *ACS Nano 7*, 428−437.

(28) Koenig, S. P., Wang, L., Pellegrino, J., and Bunch, J. S. (2012) Selective Molecular Sieving through Porous Graphene. *Nat. Nanotechnol. 7*, 728−732.

(29) Li, H., Song, Z., Zhang, X., Huang, Y., Li, S., Mao, Y., Ploehn, H. J., Bao, Y., and Yu, M. (2013) Ultrathin, Molecular-Sieving Graphene Oxide Membranes for Selective Hydrogen Separation. *Science 342*, 95−98.

(30) Joshi, R. K., Carbone, P., Wang, F. C., Kravets, V. G., Su, Y., Grigorieva, I. V., Wu, H. A., Geim, A. K., and Nair, R. R. (2014) Precise and Ultrafast Molecular Sieving through Graphene Oxide Membranes. *Science 343*, 752−754.

(31) Kim, H. W., Yoon, H. W., Yoon, S. M., Yoo, B. M., Ahn, B. K., Cho, Y. H., Shin, H. J., Yang, H., Paik, U., and Kwon, S. (2013) Selective Gas Transport Through Few-Layered Graphene and Graphene Oxide Membranes. *Science 342*, 91−95.

(32) Liu, Z., Robinson, J. T., Sun, X., Dai, H., Wang, Y., Li, Z., Hu, D., Lin, C.-T., Li, J., and Lin, Y. (2010) Aptamer/Graphene Oxide Nanocomplex for *in Situ* Molecular Probing in Living Cells. *J. Am. Chem. Soc. 132*, 9274−9276.

(33) Hummers, W. S., and Offeman, R. E. (1958) Preparation of Graphitic Oxide. *J. Am. Chem. Soc. 80*, 1339.

(34) Fan, Z., Kanchanapally, R., and Ray, P. C. (2013) Hybrid Graphene Oxide Based Ultrasensitive SERS Probe for Label-Free Biosensing. *J. Phys. Chem. Lett. 4*, 3813.

(35) Pramanik, A., Chavva, S. R., Fan, Z., Sinha, S., Nellore, B. P., and Ray, P. C. (2014) Extremely High Two-Photon Absorbing Graphene Oxide for Imaging of Tumor Cells in the Second Biological Window. *J. Phys. Chem. Lett. 5*, 2150−2154.

(36) Pramanik, A., Fan, Z., Reddy, S. C., Sinha, S. S., and Ray, P. C. (2014) Highly Efficient and Excitation Tunable Two-Photon Luminescence Platform For Targeted Multi-Color MDRB Imaging Using Graphene Oxide. *Sci. Rep. 4*, ArticleNo. 6090.

(37) Kamat, P. V. (2010) Graphene-Based Nanoarchitectures. Anchoring Semiconductor and Metal Nanoparticles on a Two-Dimensional Carbon Support. *J. Phys. Chem. Lett. 1*, 520−527.

(38) Fan, Z., Yust, B., Nellore, B. O. V., Sinha, S. S., Kanchanapally, R., Crouch, R. A., Pramanik, A., Reddy, S. C., Sardar, D., and Ray, P. C. (2014) Accurate Identification and Selective Removal of Rotavirus Using a Plasmonic−Magnetic 3D Graphene Oxide Architecture. *J. Phys. Chem. Lett. 5*, 3216−3221.

(39) Lu, W., Arumugam, S. R., Senapati, D., Singh, A. K., Arbneshi, T., Khan, S. A., Yu, H., and Ray, P. C. (2010) Multifunctional Oval Shape Gold Nanoparticle Based Selective Detection of Breast Cancer Cells Using Simple Colorimetric and Highly Sensitive Two-Photon Scattering Assay. *ACS Nano 4*, 1739−1749.

(40) King, S. H., Huh, Y. M., Kim, S., and Lee, D.-K. (2009) Isolation of RNA Aptamers Targeting HER-2-Overexpressing Breast Cancer Cells Using Cell-SELEX. *Bull. Korean Chem. Soc. 30*, 1827−1831.

(41) Lu, W., Singh, A. K., Khan, S. A., Senapati, D., Yu, H., and Ray, P. C. (2010) Gold Nano-Popcorn-Based Targeted Diagnosis, Nanotherapy Treatment, and *In Situ* Monitoring of Photothermal Destruction Response of Prostate Cancer Cells Using Surface-Enhanced Raman Spectroscopy. *J. Am. Chem. Soc. 132*, 18103−18114.

(42) Sardana, G., Jung, K., Stephan, C., and Diamandis, E. P. (2008) Proteomic analysis of conditioned media from the PC3, LNCaP, and 22Rv1 prostate cancer cell lines: Discovery and validation of candidate prostate cancer biomarkers. *J. Proteome Res. 7*, 3329−3338.

(43) Lee, Y. J., Han, S. R., Lee, S. H., Jeong, J. S., and Lee, S. W. (2012) An RNA Aptamer that Binds Carcinoembryonic Antigen Inhibits Hepatic Metastasis. *Gastroenterology 43*, 155−165.